Accepted Manuscript

High sensitivity surface plasmon resonance biosensor for detection of microRNA based on gold nanoparticles-decorated molybdenum sulfide

Wenyan Nie, Qing Wang, Xiaohai Yang, Hua Zhang, Zhiping Li, Lei Gao, Yan Zheng, Xiaofeng Liu, Kemin Wang

PII: S0003-2670(17)31061-9

DOI: 10.1016/j.aca.2017.09.015

Reference: ACA 235437

To appear in: *Analytica Chimica Acta*

Received Date: 16 May 2017

Revised Date: 21 August 2017

Accepted Date: 1 September 2017

Please cite this article as: W. Nie, Q. Wang, X. Yang, H. Zhang, Z. Li, L. Gao, Y. Zheng, X. Liu, K. Wang, High sensitivity surface plasmon resonance biosensor for detection of microRNA based on gold nanoparticles-decorated molybdenum sulfide, *Analytica Chimica Acta* (2017), doi: 10.1016/j.aca.2017.09.015.

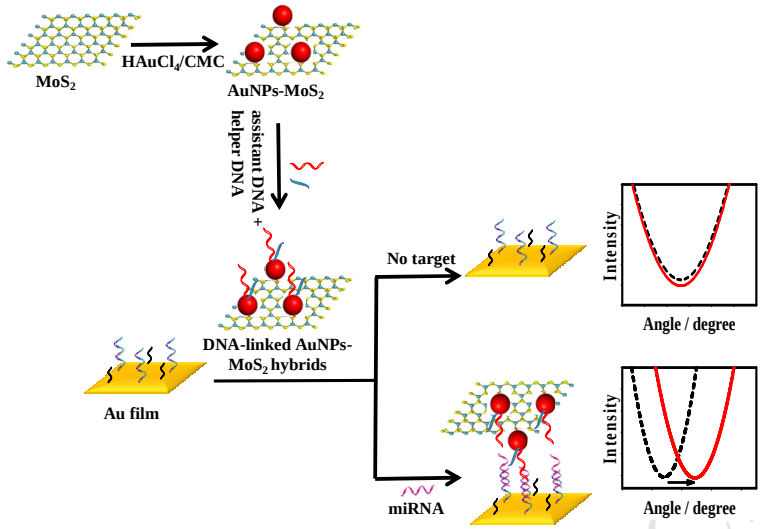

High sensitivity surface plasmon resonance biosensor for detection of microRNA based on gold nanoparticles-decorated molybdenum sulfide

Wenyan Nie, Qing Wang*, Xiaohai Yang, Hua Zhang, Zhiping Li, Lei Gao, Yan Zheng, Xiaofeng Liu, Kemin Wang*

State Key Laboratory of Chemo/Biosensing and Chemometrics, College of Chemistry and Chemical Engineering, Key Laboratory for Bio-Nanotechnology and Molecular Engineering of Hunan Province, Hunan University, Changsha 410082, China

* E-mail address: wwqq99@hnu.edu.cn kmwang@hnu.edu.cn.; Tel/Fax: +86-731-88821566.

Abstract

A high sensitive surface plasmon resonance (SPR) biosensor was proposed based on the gold nanoparticles-decorated molybdenum sulfide (AuNPs-MoS_2) for the first time. This SPR platform using the AuNPs-MoS_2 nanocomposites as signal labels for the sensitive and facile measurement of microRNA (miRNA) was executed in only two steps. At first, the thiol-modified DNA oligonucleotide probes, including a sequence complementary to the target miRNA-141, were fixed on the Au film to identify the segment sequence of target miRNA-141. Then, the assistant DNA-linked AuNPs-MoS_2 nanocomposites were used to combine with the other section of the miRNA-141. Performance of SPR biosensor was enhanced by taking advantage of the AuNPs-MoS_2 nanocomposites, thus this newly presented sensing assay exhibited high sensitivity toward miRNA with a detection limit of 0.5 fM. Furthermore, the method showed high specificity, resulting in distinguishing differences among miRNA-200 family members. Especially, the assay could also be used to detect human miRNA from cancer cells, and the results were in excellent accord with the ones obtained using qRT-PCR. What is more, this presented method could be feasible for determining miRNA in 10% human serum. This assay may provide a great potential as a miRNA quantification method in complex samples, and exert significant effect on biomedical research and clinical early diagnosis.

Keywords: Surface plasmon resonance; Gold nanoparticles-decorated molybdenum sulfide; MicroRNA

1. Introduction

The gold nanoparticles-decorated molybdenum sulfide (AuNPs-MoS_2), which the edge sites or defective sites of MoS_2 nanosheets are selectively decorated with gold nanoparticles (AuNPs) [1], not only exhibit physicochemical properties of AuNPs and MoS_2, but also usually extend additional functionalities as novel catalytic, magnetic, and optoelectronic nanomaterials [2]. For example, AuNPs-MoS_2 nanocomposites confer excellent catalytic activity as well as provide excellent electrochemical properties such as high faradic-to-capacitive current ratios, high current density, electron mobility and fast mass transport [3-7]. Because of unique physicochemical properties of the AuNPs-MoS_2 nanocomposites, they were widely applied in many sensors, such as electrochemistry sensor [8, 9], chemiluminescence biosensor [10, 11], photoluminescence sensor [12, 13], surface-enhanced Raman scattering biosensor [14, 15] and colorimetric method [16]. Among these sensors, AuNPs-MoS_2 nanocomposites generally acted as an excellent sensing substrate, since the AuNPs-MoS_2 nanocomposites could provide high surface area for capture DNA probes as well as improve their electrical conductivity and accelerate electron transfer [17, 18].

Moreover, in view that the AuNPs-MoS_2 nanocomposites generated localized surface plasmon resonance which induced strong plasmon-exciton coupling [12, 19, 20], it was speculated that AuNPs-MoS_2 nanocomposites may construct a high sensitivity SPR biosensor. However, few papers have reported that the AuNPs-MoS_2 nanocomposites were applied in SPR biosensor.

As an extension of the previous work of our group [21], a sensitive and simple SPR biosensor based on AuNPs-MoS_2 nanocomposites was proposed for the detection of microRNA (miRNA). Compared to the previous work [21], the synthesis of

AuNPs-MoS_2 nanocomposites was straightforward. Since the MoS_2 nanosheet was used as reducing agent, so the synthesis of AuNPs-MoS_2 nanocomposites need not any additional reduced agents. Especially, the AuNPs-MoS_2 nanocomposites were used in SPR sensors for the first time. The principle of AuNPs-MoS_2 nanocomposites-based SPR (AuNPs/MoS_2-SPR) biosensor was illustrated in Fig. 1. Thiol-modified probe including a sequence complementary to the target miRNA, was first immobilized on the Au film and used as capture DNA. In the presence of target miRNA-141, DNA-linked AuNPs-MoS_2 nanocomposites were served as signal labels, and a sandwich structure was formed on the SPR sensing surface. There were at least three probable causes. Firstly, the SPR signal was enhanced by localized plasmon of AuNPs and the surface plasmon wave associated with Au film generated the electronic coupling [22, 23]. Secondly, MoS_2 which loaded a large amount of AuNPs could significantly enhance SPR signal compared to gold nanoparticles. Thirdly, the photoexcited excitons could be used to active control of SPR in AuNPs-MoS_2 nanocomposites, resulting in the enhancement of SPR signal [24, 25]. With the amplification of AuNPs-MoS_2 nanocomposites, an extremely low limit of detection was reached toward miRNA-141. Interestingly, differing from previous work [8, 9, 15], this work considered AuNPs-MoS_2 nanocomposites as signal probes. More importantly, this AuNPs/MoS_2-SPR biosensor performed in only two steps and showed high sensitivity, excellent selectivity and good reproducibility. This work had great potential for practical application in clinical diagnosis and biomedical research.

Fig. 1. positioned here

2. Experimental

2.1. Materials/ Reagents

Chloroauric acid ($HAuCl_4 \cdot 4H_2O$) was obtained from Sinopharm Chemical Reagent Co., Ltd. (Beijing, China). MoS_2 nanosheet solution (1 mg L^{-1}) was purchased from XFNANO Materials Tech Co., Ltd. (Nanjing, China). Sodium carboxymethyl cellulose (CMC, 800−1200 mPa·s) was purchased from Aladdin reagent Co., Ltd. (Shanghai, China). 6-Mercapto-1-hexanol (MCH) was provided from Sigma (U.S.A). All nucleic acid probes were synthesized by Shanghai Sangon Biotechnology Co. (Shanghai, China) and were listed in Table 1. All reagents used in the experiments were prepared by ultrapure water (18.2 MΩ cm). DNA probes and miRNA were dissolved into PBS buffer (0.01M, pH 7.4) containing 100 mM NaCl before use. In order to keep an RNase-free environment, 0.1% diethyl pyrocarbonate (DEPC) were used to dispose of all solutions, then all solutions were autoclaved.

Table 1. positioned here

2.2. Preparation AuNPs-MoS_2 and DNA-linked AuNPs-MoS_2 nanocomposites

AuNPs-MoS_2 nanocomposites were synthesized by hydrothermal synthesis method [2, 26]. In a typical synthesis, CMC (400 μL, 50 mM) and $HAuCl_4 \cdot 4H_2O$ (197 μL, 24.28 mM) were immediately mixed with MoS_2 nanosheets (5 mL, 0.08 mg/mL) aqueous dispersion under vigorous stirring. Then, the above mixture was heated to 40 °C for 5 min. Finally, the product of AuNPs-MoS_2 nanocomposites was centrifuged and stored at 4 °C for further use.

According to the literature with minor modifications [27], DNA-linked AuNPs-MoS_2 nanocomposites were prepared. Firstly, assistant DNA (4.5 μL, 100 μM) and helper DNA (4.5 μL, 100 μM) were added to 441 μL AuNPs-MoS_2

nanocomposites solution for 16 h at 4 °C, and then the solution was mixed with 500 mM NaCl solution (300 μL, pH 7.0, 50 mM PBS) for aging 40 h at 4 °C. Helper DNA can protect the AuNPs-MoS_2 from being aggregated in salt solution due to strong interparticle electrostatic repulsion [28, 29]. Next, the DNA-linked AuNPs-MoS_2 nanocomposites were centrifuged (30 min, 13,000 rpm) to remove excess reagents. The supernatant was discarded and the precipitate was washed with 100 mM NaCl solution (pH 7.0, 10 mM PBS). After a second centrifugation, the precipitate was dispersed in 100 mM NaCl solution (800μL, pH 7.0, 10 mM PBS).

2.3. The fabrication of SPR sensor

The Au film was cleaned according to our previous work [30-32]. The Au film was docked into EC-SPR1010 device (Changchun Dingcheng Technology, China). DNA probes (5 μM) in PBS (0.01 M, pH 7.4) was dripped to the Au film for 3 h incubation. Then it was washed by PBS (0.01 M, pH 7.4) to remove excess probe. MCH (1 mM) was employed to block the gold film for 30 min. In addition, thiol-modified capture DNA probes were also raised off the surface by MCH [33]. Finally, the Au film was washed by with PBS (0.01 M, pH 7.4). The sensor chip was obtained.

2.4. MiRNA detection protocol

At room temperature, detection of miRNA-141 was conducted by exposing the sensor chip to different concentration of miRNA-141 solution or tumor cell extractions or 10 % human serum which contained miRNA for 60 min, and then the resonance angle was recorded after washing with 10 mM PBS repeatedly, i.e. target

miRNA-141 was detected by direct hybridization. Next, DNA-linked AuNPs or DNA-linked AuNPs-MoS_2 was added for reacting about 50 min at room temperature, and the resonance angle was recorded after washing with 10 mM PBS repeatedly, i.e. target miRNA-141 was detected by AuNPs amplified SPR or AuNPs/MoS_2-SPR. Finally, 0.1% SDS/10 mM NaOH was introduced for 5 min to regenerate the sensor chip for further use.

2.5. Cell extractions and qRT-PCR analysis

Four human cancer cell lines, including prostate carcinoma cell lines (22Rv1), hepatocellular carcinoma cell lines (SMMC-7721), colon cancer cell lines (LoVo) and cervical cancer cell lines (HeLa), were employed to prepare the biological samples. The cell culture and corresponding cell lysates were prepared according to our previous work [21, 34]. The total RNA, including miRNA, was extracted from the human cancer cell lines using a Trizol reagent (Sangon Co.Ltd, Shanghai, China). The concentrated and pure RNA was divided into two equal parts for the detection using qRT-PCR (Sangon Co. Ltd, Shanghai, China) and the AuNPs/MoS_2-SPR biosensor. The detection of target miRNA-141 in cell extractions followed the above procedures.

3. Results and discussion

3.1. Characterization of AuNPs-MoS_2 nanocomposites and DNA-linked AuNPs-MoS_2 nanocomposites

The as-prepared AuNPs-MoS_2 nanocomposites were characterized using Tecnai F20 transmission electron microscopy (FEI, Netherlands). As shown in Fig. 2A, the

AuNPs with a diameter around 10 nm were decorated on the surface of MoS_2 nanosheets, suggesting that the AuNPs-MoS_2 nanocomposites were successfully prepared. Fig. 2B showed the elemental composition of the synthesized AuNPs-MoS_2 nanocomposites was characterized by using scanning transmission electron microscope-energy dispersive X-ray spectroscopy (STEM-EDX) maps. It was found that the signals from three elements, Au (Fig. 2B, curve b), Mo (Fig. 2B, curve c) and S (Fig. 2B, curve d) were detected, implying the synthesis of AuNPs-MoS_2 nanocomposites. In addition, the AuNPs-MoS_2 nanocomposites were also characterized using UV-2600 spectrophotometer (Shimadzu, Japan). As shown in Fig. 2C, one characteristic absorption peaks of MoS_2 nanosheets were located at 304 nm (Fig. 2C, curve a). When $HAuCl_4$ was added into chemically exfoliated MoS_2, the absorption peak of Au^{3+} at around 289 nm (Fig. 2C, curve b) decreased significantly and a new absorption peak corresponding to the AuNPs at around 537 nm emerged. Meanwhile, obvious absorption peak at 251 nm corresponding to the MoS_2 was observed in the mixture solution, suggesting the synthesis of AuNPs-MoS_2 nanocomposites (Fig. 2C, curve c).

The structure of MoS_2 and AuNPs-MoS_2 nanocomposites was characterized using Powder X-ray diffraction (XRD) (D/MAX 2500, Japan). As shown in Fig. 2D, a diffraction peak located at about 14.40° for MoS_2 nanosheet, which was matched with the (001) index of 1T-MoS_2 [35, 36]. After modification, strong diffraction peaks emerged at 40.0° for AuNPs-MoS_2 nanocomposites, which can be assigned to the (111) planes of Au (JCPDS no. 04-0784) [37, 38]. The results indicated the successful

formation of AuNPs-MoS_2 nanocomposites.

The structure and composition of the AuNPs-MoS_2 nanocomposites were investigated by X-ray Photoelectron Spectroscopy (XPS) (K-Alpha 1063, England). It had reported that a trigonal orismatic (2H) and an octahedral (1T) configuration of MoS_2 could coexist during the lithium intercalation-exfoliation process [36-38]. As shown in Fig. 2E, the binding energy peaks of MoS_2 nanosheet was fitted into three groups: (1) two larger peaks located near 232.6 eV and 229.3 eV, respectively, which corresponding to Mo^{4+} $3d_{3/2}$ and Mo^{4+} $3d_{5/2}$ of 2H-MoS_2; (2) the two peaks located around 231.8 eV and 228.6 eV could be assigned to Mo^{4+} $3d_{3/2}$ and Mo^{4+} $3d_{5/2}$ of 1T-MoS_2; (3) relative weak peaks located at 235.2 eV and 231.8 eV are sign of Mo 3d peaks with higher oxidation state (Mo^{6+}), which may originate from the partial oxidation of Mo atoms at the edges or defects of the MoS_2 nanosheet during chemical exfoliation and preparation of AuNPs-MoS_2 [5, 37, 38], The binding energy for S $2p_{3/2}$ and S $2p_{1/2}$ were 162.3 eV and 163.5 eV, respectively (Fig. 2F). Two peaks located at about 87.2 eV and 83.5 eV can be ascribed to Au $4f_{5/2}$ and Au $4f_{7/2}$, respectively (Fig. 2G). The XPS results further confirmed the existence of the AuNPs-MoS_2 nanocomposites.

Fig. 2. positioned here

DNA-linked AuNPs-MoS_2 nanocomposites were also characterized using UV-2600 spectrophotometer (Shimadzu, Japan). As shown in Fig. S1 (Supporting Information), on the absorption spectra of AuNPs-MoS_2 nanocomposites and DNA-linked AuNPs-MoS_2 nanocomposites, the characteristic absorption peak of

AuNPs was 537 nm (Fig. S1 (Supporting Information), curve a) and 540 nm (Fig. S1 (Supporting Information), curve b) respectively, confirming that AuNPs-MoS_2 nanocomposites were labeled with assistant DNA.

3.2. The feasibility

The feasibility of this method was first investigated. As shown in Fig. 3, when 50 pM miRNA-141 was added and incubated with capture DNA modified Au film, SPR spectrum shifted from curve 1 to curve 2 and small resonance angle shift ($\Delta\theta$ = 0.0126°) was observed. Then DNA-linked AuNPs-MoS_2 nanocomposites were added, SPR spectrum shifted from curve 2 to curve 3 and an obvious resonance angle shift (0.2632°) was observed, suggesting that the DNA-linked AuNPs-MoS_2 nanocomposites were captured on the Au film through hybridization. When 0.1% SDS/10 mM NaOH was introduced for 5 min, SPR spectrum shifted from curve 3 to curve 4. The resonance angle of curve 4 was basically consistent with that of curve 1, implying that the sensor chip could be regenerated. The results showed that miRNA-141 could be detected using SPR biosensor based on AuNPs-MoS_2 amplification strategy.

Fig. 3. positioned here

3.3. Optimization of the experimental conditions

Different experimental parameters, such as the surface density of the capture probe on the Au film and the incubation time of miRNA-141 could influence the performance of the detection system. To achieve optimal sensing performance, the effects of these factors were investigated.

The effect of the Au film with different surface densities of the capture probe was first investigated. The surface density of the capture probe on the Au film was quantitatively measured with chronocoulometry, as previously described [39]. As shown in Fig. 4A, different surface coverage (1.75×10^{12} molecules per cm^2, 4.85×10^{12} molecules per cm^2, and 1.06×10^{13} molecules per cm^2) was obtained through the incubation of the Au film with 1 μM, 5 μM, and 10 μM of the capture probe, respectively. The largest $\Delta\theta$ could be obtained at 5 μM capture probe (4.85×10^{12} molecules per cm^2). Presumably, the low-density DNA surface captured few target strands and the high-density DNA surface decreased the hybridization efficiency, resulting in the decrease of $\Delta\theta$. Therefore, a 5 μM capture probe was chosen for the following experiments.

In addition, the effect of incubation time of miRNA-141 and the capture probe on Au film surface was investigated. As shown in Fig. 4B, SPR signal increased with the increase of time, and then reached a plateau at 60 min. Therefore, 60 min was selected as the optimal incubation time of miRNA-141.

Fig. 4. positioned here

3.4. Analytical performance of miRNA-141 detection

Different concentrations of miRNA-141 were also successively measured by the proposed AuNPs/MoS_2-SPR biosensor. As shown in Fig. 5A, in the absence of miRNA-141, SPR response hardly changed in blank solution. As the miRNA-141 concentrations rose from 0 to 50 pM, SPR response gradually increased. However, as shown in Fig. S2 (Supporting Information), when the miRNA-141 concentrations rose

from 0 to 50 pM, SPR response slowly increased without adding DNA-linked AuNPs-MoS_2 nanocomposites. The reason may be that the increased quantity of DNA-linked AuNPs-MoS_2 nanocomposites was captured on Au film. Fig. 5B illustrated that the relation between the shift of resonance angle ($\Delta\theta$) and the concentration of miRNA-141 of three methods (i.e. direct hybridization measurement, AuNPs amplified SPR and AuNPs/MoS_2-SPR). Since a shift of resonance angle larger than 0.0015° was regarded as signal for the SPR instrument, it was estimated that this proposed AuNPs/MoS_2-SPR (Fig. 5B, curve c) approach allowed detection of miRNA with the limit of detection down to 0.5 fM. In addition, direct hybridization measurement (Fig. 5B, curve a) and AuNPs amplified SPR (Fig. 5B, curve b) method allowed the minimum target concentrations detected were 100 pM and 1 pM respectively. Therefore, AuNPs-MoS_2 nanocomposites could significantly enhance SPR signal compared to pure AuNPs. This result was similar to that of the graphene oxide–gold nanoparticles hybrids-based SPR biosensor in our previous work [21]. One possibility is that MoS_2 nanosheet as a graphene analogue has distinct similarities compared to graphene such as 2D ultrathin atomic layer structure and high surface area [2]. Moreover, to further evaluate high amplification effect of the AuNPs/MoS_2-SPR biosensor, its detection limit was compared to the previous works in Table 2. The results showed the high sensitivity of the AuNPs/MoS_2-SPR biosensor.

Table 2. positioned here

Next, miRNA-141, miRNA-200a, miRNA-429, let-7d and random miRNA were

used to investigate the selectivity capability of AuNPs/MoS_2-SPR biosensor. The change of SPR response was hardly observed in the absence of miRNA-141 (Fig. 5B). As shown in Fig. 5C, as the concentration increased, there was almost no change in resonance angle for let-7d and random miRNA. Δθ increased slightly in case of miRNA-429 and miRNA-200a. However, Δθ increased obviously in case of miRNA-141. Take 10 pM miRNA as example, Δθ was 0.1933° for miRNA-141, which was more than five times larger than that of miRNA-429 and four times larger than that of miRNA-200a. The results indicated the good selectivity of the AuNPs/MoS_2-SPR for miRNA-141 detection.

The reproducibility of the sensor chip was investigated. After a sample was measured, 0.1% SDS/10 mM NaOH was used to regenerate the Au film surface for the next round of analysis. As shown in Fig. 5D, when 10 pM miRNA-141 was detected using the AuNPs/MoS_2-SPR biosensor, no significant signal degradation was observed during the 6 cycles and the standard deviation was about 1.2% (n=6), suggesting that this SPR biosensor exhibited good reproducibility.

Fig 5. positioned here

3.5. Application of the biosensor in biological sample

To further confirm the application of the AuNPs/MoS_2-SPR biosensor in biological analysis, the cell lysates from four human cancer cell lines, including 22Rv1, SMMC-7721, LoVo and HeLa, were tested. The relative expression levels which were employed to stand for the levels of miRNA-141, referred to the expression ratio of miRNA-141 in the target cell lines versus that in the LoVo cell

lines. As shown in Fig. 6A, the cell lysates from 22Rv1 cell lines had higher concentration of miRNA-141 than that from LoVo cell lines. Compared to LoVo cell lines, concentration of miRNA-141 obviously decreased in 7721 cell lines and HeLa cell lines. The results clearly demonstrated the varied contents of miRNA-141 in the cells, which were in good agreement with reported literature [21, 45]. In addition, to assess the reliability of this AuNPs/MoS_2-SPR biosensor, qRT-PCR and the AuNPs/MoS_2-SPR biosensor were used specifically to detect the relative expression levels of miRNA-141 in cell lysates. The results obtained by the AuNPs/MoS_2-SPR biosensor in excellent agreement with the ones obtained qRT-PCR. The results showed that the AuNPs/MoS_2-SPR biosensor held a great potential in the early clinic diagnosis with accuracy and reliability.

The AuNPs/MoS_2-SPR biosensor was also applied to measure miRNA-141 in human serum. The human normal serum (which does not contain miRNA in detectable quantity) was diluted 10 times [46, 47], and first treated using the RNase inhibitor. Then, miRNA-141 of known different concentration were added into the serum sample to obtain miRNA-141 spiked serum sample. Next, after the miRNA-141 spiked serum samples were centrifuged to remove the macromolecules using the centrifugal filtration devices (30 K), the spiked serum samples were detected. As shown in Fig. 6B, the signal caused by miRNA-141 in 10% human serum was similar to that caused by miRNA-141 in the PBS. The results suggested that the other components of the serum did not influence the measuring properties of the proposed biosensor.

Fig. 6. positioned here

4. Conclusion

In summary, a sensitive SPR biosensor for detecting miRNA was fabricated based on AuNPs-MoS_2 nanocomposites. On the basis of signal amplification of AuNPs-MoS_2 nanocomposites, the AuNPs/MoS_2-SPR biosensor exhibited high sensitivity toward target miRNA with a detection limit of 0.5 fM. Moreover, the developed biosensor showed high specificity, acceptable reproducibility and precision, and could be applied to monitor human miRNA from cancer cells. The results obtained using the AuNPs/MoS_2-SPR biosensor were in accord with the ones obtained using qRT-PCR. In addition, this presented method could be feasible for determining miRNA in 10% human normal serum. More importantly, the assay was enzyme-free and cost-effective. These distinctive features indicate that our method will be a promising miRNA detection assay in clinical diagnosis and disease treatment.

Acknowledgments

This work was supported by the National Natural Science Foundation of China (Grants 21375034, 21675047 and 21190040) and Natural Science Foundation for Distinguished Young Scholars of Hunan Province (Grant 2016JJ1008).

References

[1] Y.M. Shi, J.K. Huang, L.M. Jin, Y.T. Hsu, S.F. Yu, L.J. Li, H.Y. Yang, Selective

decoration of Au nanoparticles on monolayer MoS_2 single crystals, Sci. Rep. 3 (2013) 1839.

[2] S. Su, C. Zhang, L.H. Yuwen, J. Chao, X.L. Zuo, X.F. Liu, C.Y. Song, C.H. Fan, L.H. Wang, Creating SERS hot spots on MoS_2 nanosheets with in situ grown gold nanoparticles, ACS Appl. Mater. Interfaces 6 (2014) 18735–18741.

[3] J.Y. Kim, S. Byun, A.J. Smith, J. Yu, J.X. Huang, Enhanced electrocatalytic properties of transition-metal dichalcogenides sheets by spontaneous gold nanoparticle decoration, J. Phys. Chem. Lett. 4 (2013) 1227–1232.

[4] O. Parlak, A. İncel, L. Uzun, A.P.F. Turner, A. Tiwari, Structuring Au nanoparticles on two-dimensional MoS_2 nanosheets for electrochemical glucose biosensors, Biosens. Bioelectron. 89 (2017) 545–550.

[5] Y. Shi, J. Wang, C. Wang, T.T. Zhai, W.J. Bao, J.J. Xu, X.H. Xia, H.Y. Chen, Hot electron of Au nanorods activates the electrocatalysis of hydrogen evolution on MoS_2 nanosheets, J. Am. Chem. Soc. 137 (2015) 7365–7370.

[6] S. Su, M. Zou, H. Zhao, C.F. Yuan, Y.N. Xu, C. Zhang, L.H. Wang, C.H. Fan, L.H. Wang, Shape-controlled gold nanoparticles supported on MoS_2 nanosheets: synergistic effect of thionine and MoS_2 and their application for electrochemical label-free immunosensing. Nanoscale 7 (2015) 19129–19135.

[7] P. Zhang, M. Fujitsuka, T. Majima, Hot electron-driven hydrogen evolution using anisotropic gold nanostructure assembled monolayer MoS_2, Nanoscale 9 (2017) 1520.

[8] S. Su, H.F. Sun, W.F. Cao, J. Chao, H.Z. Peng, X.L. Zuo, L.H. Yuwen, C.H. Fan, L.H. Wang, Dual-target electrochemical biosensing based on DNA structural

switching on gold nanoparticle-decorated MoS_2 nanosheets, ACS Appl. Mater. Interfaces 8 (2016) 6826–6833.

[9] Y.Y. Yang, H. Zhang, C.S. Huang, D.P. Yang, N.Q. Jia, Electrochemical non-enzyme sensor for detecting clenbuterol (CLB) based on MoS_2-Au-PEI-hemin layered nanocomposites, Biosens. Bioelectron. 9 (2017) 461–467.

[10] Y.M. Liu, M. Zhou, Y.Y. Liu, G.F. Shi, J.J. Zhang, J.T. Cao, K.J. Huang, Y.H. Chen, Fabrication of electrochemiluminescence aptasensor based on in situ growth of gold nanoparticles on layered molybdenum disulfide for sensitive detection of platelet-derived growth factor-BB, RSC Adv. 4 (2014) 22888–22893.

[11] X. Wang, W.P. Deng, L. Shen, M. Yan, S.G. Ge, J.H. Yu, A sensitive quenched electrochemiluminescent DNA sensor based on the catalytic activity of gold nanoparticle functionalized MoS_2, New J. Chem. 39 (2015) 8100–8107.

[12] U. Bhanu, M.R. Islam, L. Tetard, S.I. Khondaker, Photoluminescence quenching in gold-MoS_2 hybrid nanoflakes, Sci. Rep. 4 (2014) 5575.

[13] Y. Li, J.D. Cain, E.D. Hanson, A.A. Murthy, S.Q. Hao, F.Y. Shi, Q.Q. Li, C. Wolverton, X.Q. Chen, V.P. Dravid, Au@MoS_2 core–shell heterostructures with strong light-matter interactions, Nano Lett. 16 (2016) 7696−7702.

[14] X.J. Yu, T. Shiraki, S.C. Yang, B.J. Ding, N. Nakashima, Synthesis of porous gold nanoparticle/MoS_2 nanocomposites based on redox reactions, RSC Adv. 5 (2015) 86558–86563.

[15] H.Q. Zhou, F. Yu, C.F. Guo, Z.P. Wang, Y.C. Lan, G. Wang, Z.Y. Fang, Y. Liu, S. Chen, L.F. Sun, Well-oriented epitaxial gold nanotriangles and bowties on MoS_2 for

surface-enhanced Raman scattering, Nanoscale 7 (2015) 9153–9157.

[16] N.R. Nirala, S. Pandey, A. Bansal, V.K. Singh, B. Mukherjee, P.S. Saxena, A. Srivastava, Different shades of cholesterol: Gold nanoparticles supported on MoS_2 nanoribbons for enhanced colorimetric sensing of free cholesterol, Biosens. Bioelectron. 74 (2015) 207–213.

[17] S.Y. Cho, H.J. Koh, H.W. Yoo, J.S. Kim, H.T. Jung, Tunable volatile-organic-compound sensor by using Au nanoparticle incorporation on MoS_2, ACS Sens. 2 (2017) 183–189.

[18] H.L. Shuai, K.J. Huang, Y.X. Chen, L.X. Fang, M.P. Jia, Au nanoparticles/hollow molybdenum disulfide microcubes based biosensor for microRNA-21 detection coupled with duplex-specific nuclease and enzyme signal amplification, Biosens. Bioelectron. 89 (2017) 989–997.

[19] J.S. Miao, W.D. Hu, Y.L. Jing, W.J. Luo, L. Liao, A.L. Pan, S.W. Wu, J.X.; Chen, X.S. Cheng, W. Lu, Surface plasmon-enhanced photodetection in few layer MoS_2 phototransistors with Au nanostructure arrays, Small 11 (2015) 2392–2398.

[20] P. Zuo, L. Jiang, X. Li, B. Li, Y.D. Xu, X.S. Shi, P. Ran, T.B. Ma, D.W. Li, L.T. Qu, Shape-controllable gold nanoparticles-MoS_2 hybrids prepared by tuning edge-active sites and surface structures of MoS_2 via temporally shaped femtosecond pulses, ACS Appl. Mater. Interfaces 9 (2017) 7447−7455.

[21] Q. Wang, Q. Li, X.H. Yang, K.M. Wang, S.S. Du, H. Zhang, Y.J. Nie, Graphene oxide–gold nanoparticles hybrids-based surface plasmon resonance for sensitive detection of microRNA. Biosens. Bioelectron. 77 (2016) 1001–1007.

[22] S. Fang, H.J. Lee, A.W. Wark, R.M. Corn, Attomole microarray detection of microRNAs by nanoparticle-amplified SPR imaging measurements of surface polyadenylation reactions, J. Am. Chem. Soc. 128 (2006) 14044–14046.

[23] W. Hu, G. He, H. Zhang, X. Wu, J. Li, Z. Zhao, Y. Qiao, Z. Lu, Y. Liu, C.M. Li, Polydopamine-functionalization of graphene oxide to enable dual signal amplification for sensitive surface plasmon resonance imaging detection of biomarker, Anal. Chem. 86 (2014) 4488-4493.

[24] S. Zu, B. Li, Y.J. Gong, Z.W. Li, P.M. Ajayan, Z.Y. Fang, Active control of plasmon–exciton coupling in MoS_2-Ag hybrid nanostructures. Adv. Opt. Mater. 4 (2016) 1463–1469.

[25] T. Borzda, C. Gadermaier, N. Vujicic, P. Topolovsek, M. Borovsak, Charge Photogeneration in Few-Layer MoS_2, Adv. Funct. Mater. 25 (2015) 3351–3358.

[26] J. Chao, M. Zou, C. Zhang, H. Sun, D. Pan, H. Pei, S. Su, L.H. Yuwen, C.H. Fan, L.H. Wang, A MoS_2–based system for efficient immobilization of hemoglobin and biosensing applications. Nanotechnol. 26 (2015) 274005.

[27] Q. Wang, R.J. Liu, X.H. Yang, K.M. Wang, J.Q. Zhu, L.L. He, Q. Li, Surface plasmon resonance biosensor for enzyme-free amplified microRNA detection based on gold nanoparticles and DNA supersandwich, Sens. Actuators, B 223 (2016) 613–620.

[28] R. Elghanian, J. J. Storhoff, R. C. Mucic, R. L. Letsinger, C. A. Mirkin, Selective colorimetric detection of polynucleotides based on the distance-dependent optical properties of gold nanoparticles. Science 277 (1997), 1078-1081.

[29] S. Song, Z. Liang, J. Zhang, L. Wang, G. Li, C. Fan, Gold-nanoparticle-based multicolor nanobeacons for sequence-specific DNA analysis. Angew. Chem. 121 (2009), 8826-8830.

[30] Y.N. Chou, F. Sun, H.C. Hung, P. Jain, A. Sinclair, P. Zhang, T. Bai, Y. Chang, T.C. Wen, Q. Yu, S.Y. Jiang, Ultra-low fouling and high antibody loading zwitterionic hydrogel coatings for sensing and detection in complex media. Acta Biomater. 40 (2016) 31–37.

[31] R.J. Liu, Q. Wang, Q. Li, X.H. Yang, K.M. Wang, W.Y. Nie, Surface plasmon resonance biosensor for sensitive detection of microRNA and cancer cell using multiple signal amplification strategy, Biosens. Bioelectron. 87 (2017) 433–438.

[32] B. Wu, R. Jiang, Q. Wang, J. Huang, X.H. Yang, K.M. Wang, W.S. Li, N.D. Chen, Q. Li, Detection of C-reactive protein using nanoparticle-enhanced surface plasmon resonance using an aptamer-antibody sandwich assay, Chem. Commun. 52 (2016) 3568–3571.

[33] T.M. Herne, M.J. Tarlov, Characterization of DNA probes immobilized on gold surfaces, J. Am. Chem. Soc. 119 (1997) 8916–8920.

[34] H. Zhang, Q. Wang, X.H. Yang, K.M. Wang, Q. Li, Z.P. Li, L. Gao, W.Y. Nie, Y. Zheng, An isothermal electrochemical biosensor for the sensitive detection of microRNA based on a catalytic hairpin assembly and supersandwich amplification, Analyst 142 (2017) 389–396.

[35] C. Tan, H. Zhang, Two-dimensional transition metal dichalcogenide nanosheet-based composites, Chem. Soc. Rev. 2015, 44 (2015) 2713-2731.

[36] W. Zhou, Z. Yin, Y. Du, X. Huang, Z. Zeng, Z. Fan, H. Liu, J. Wang, H. Zhang, Synthesis of few-layer MoS_2 nanosheet-coated TiO_2 nanobelt heterostructures for enhanced photocatalytic activities, Small 9 (2013), 140-147.

[37] L.H. Yuwen, F. Xu, B. Xue, Z. Luo, Q. Zhang, B. Bao, S. Su, L. Weng, W. Huang, L. Wang, General synthesis of noble metal (Au, Ag, Pd, Pt) nanocrystal modified MoS_2 nanosheets and the enhanced catalytic activity of Pd–MoS_2 for methanol oxidation, Nanoscale 6 (2014), 5762-5769.

[38] S. Su, C. Zhang, L.H Yuwen, X. F Liu, L.H. Wang, C.H. Fan and L.H. Wang, Uniform Au@ Pt core–shell nanodendrites supported on molybdenum disulfide nanosheets for the methanol oxidation reaction, Nanoscale 8 (2016), 602-608.

[39] A. B. Steel, T. M. Herne and M. J. Tarlov, Electrochemical quantitation of DNA immobilized on gold. Anal. Chem. 70 (1998), 4670–4677.

[40] K.H. Hao, Y. He, H.T. Lu, S.T. Pu, Y.N. Zhang, H.F. Dong, X.J. Zhang, High-sensitive surface plasmon resonance microRNA biosensor based on streptavidin functionalized gold nanorods-assisted signal amplification, Anal. Chim. Acta 954 (2017) 114–120.

[41] X.J. Ding, Y.R. Yan, S.Q. Li, Y. Zhang, W. Cheng, Q. Cheng, S.J. Ding, Surface plasmon resonance biosensor for highly sensitive detection of microRNA based on DNA super-sandwich assemblies and streptavidin signal amplification Anal. Chim. Acta 874 (2015) 59–65.

[42] H. Vaisocherová, H. Šípová, I. Víšová, M. Bocková, T. Špringer, M.L. Ermini, X. Song, Z. Krejčík, L. Chrastinová, O. Pastva, Rapid and sensitive detection of multiple

microRNAs in cell lysate by low-fouling surface plasmon resonance biosensor, Biosens. Bioelectron. 70 (2015) 226–231.

[43] W.J. Zhou, Y.L. Chen, R.M. Corn, Ultrasensitive microarray detection of short RNA sequences with enzymatically modified nanoparticles and surface plasmon resonance imaging measurements, Anal. Chem. 83 (2011) 3897–3902.

[44] N. Nasheri, J. Cheng, R. Singaravelu, P. Wu, M.T. McDermott, J.P. Pezacki, An enzyme-linked assay for the rapid quantification of microRNAs based on the viral suppressor of RNA silencing protein p19, Anal. Biochem. 412 (2011) 165–172.

[45] B.C. Yin, Y.Q. Liu, B.C. Ye, One-step, multiplexed fluorescence detection of microRNAs based on duplex-specific nuclease signal amplification, J. Am. Chem. Soc. 134 (2012) 5064–5067.

[46] H.V. Tran, B. Piro, S. Reisberg, L.D. Tran, H.T. Duc, M.C. Pham, Label-free and reagentless electrochemical detection of microRNAs using a conducting polymer nanostructured by carbon nanotubes: application to prostate cancer biomarker miR-141, Biosens. Bioelectron. 49 (2013) 164–169.

[47] E. Kim, P.D. Howes, S.W. Crowder, M.M. Stevens, Multi-amplified sensing of microRNA by a small DNA fragment-driven enzymatic cascade reaction. ACS Sens. 2 (2017) 111–118.

Table Captions

Table 1. Sequences of all nucleic acid probes used.

Table 2. Detection performance comparison of our strategy with other SPR methods.

Figure Captions

Fig. 1. The schematic illustration of the SPR biosensor based on the AuNPs-MoS_2 nanocomposites amplification.

Fig. 2. (A) TEM images of AuNP-MoS_2 nanocomposites. (B) Scanning transmission electron microscope-High angle annular dark-field (STEM-HAADF) image (a), Scanning transmission electron microscope-Energy dispersive X-ray spectroscopy (STEM-EDX) maps in Au Lα1 (b), S Kα1 (c), and Mo Kα1 (d) signals. (C) UV–Vis adsorption spectra of MoS_2 (a), $HAuCl_4$ (b) and AuNPs-MoS_2 nanocomposites (c). (D) XRD pattern of MoS_2 (a) and AuNPs-MoS_2 nanocomposites (b). X-ray Photoelectron Spectroscopy (XPS) spectra of AuNPs-MoS_2 nanocomposites in the Mo 3d (E), S 2p (F), and Au 4f (G) region.

Fig. 3. SPR spectra of (1) capture DNA modified Au film; (2) hybridization with 50 pM miRNA-141; (3) reaction with the DNA-linked AuNPs-MoS_2; (4) regeneration.

Fig. 4. Optimization of the experimental conditions. Effects of (A) surface density, (B) the incubation time of miRNA-141 (50 pM). The error bars represent the standard deviation of the three independent measurements. When one parameter changed, the others were under their optimal conditions.

Fig. 5. (A) SPR spectra of different concentrations of miRNA-141. (B) The relationship between Δθ and miRNA-141 concentrations by using different sensing

strategies. Error bars showed the standard deviation of measurement taken from three experiments. Direct hybridization measurement (a), AuNPs amplified SPR (b), and AuNPs/MoS_2-SPR (c). (C) Selectivity investigation of the AuNPs/MoS_2-SPR biosensor. Error bars showed the standard deviation of measurement taken from three experiments. (D) Reproducibility investigation of the AuNPs/MoS_2-SPR biosensor. The sensor chip was regenerated by introducing 0.1% SDS/10 mM NaOH for 5 min.

Fig. 6. (A) Paired comparison of the miRNA-141 levels detected in the total RNA isolated from four types of human cancer cell lines using qRT-PCR (red histogram) or the proposed biosensor (green histogram). Relative signal intensity was based on the expression ratio of miRNA-141 in the target cell lines versus that in the LoVo cell lines. (B) Detection of miRNA-141 in 10% human serum (red histogram) and buffer (green histogram). Error bars showed the standard deviation of measurement taken from three experiments.

Table 1. Sequences of all nucleic acid probes used.

Name	**Sequence (5′–3′)**
Capture DNA	AGACAGTGTTATTTTTTTTTT-SH
Assistant DNA	SH-TTTTTTTTTTTTTCCATCTTTACC
Helper DNA	SH-TTTTTTTTTTTTT
miRNA-141	UAACACUGUCUGGUAAAGAUGG
miRNA-429	UAAUACUGUCUGGUAAAACCGU
miRNA-200a	UAACACUGUCUGGUAACGAUGU
let-7d	AGAGGUAGUAGGUUGCAUAGUU
Radom miRNA	N_{22}

Table 2. Detection performance comparison of our strategy with other SPR methods.

SPR platform	Amplification strategy	Detection limit	Reference
Biacore X	Streptavidinylated gold nanorods amplification	0.045 pM	[40]
Biacore X	Streptavidin and supersandwich amplification	9 pM	[41]
SPRimager	AuNPs and polymerase amplification	10 fM	[22]
SPRimager	AuNPs amplification	0.5 pM	[42]
SPR imaging	SiNPs and polymeras amplification	100 fM	[43]
SPR imaging	Protein p19 amplification	1 fM	[44]
SPR	multiple amplification strategy	0.6 fM	[31]
SPR	GO-AuNPs hybrids amplification	1 fM	[21]
SPR	AuNP-MoS_2 hybrids amplification	0.5 fM	This work

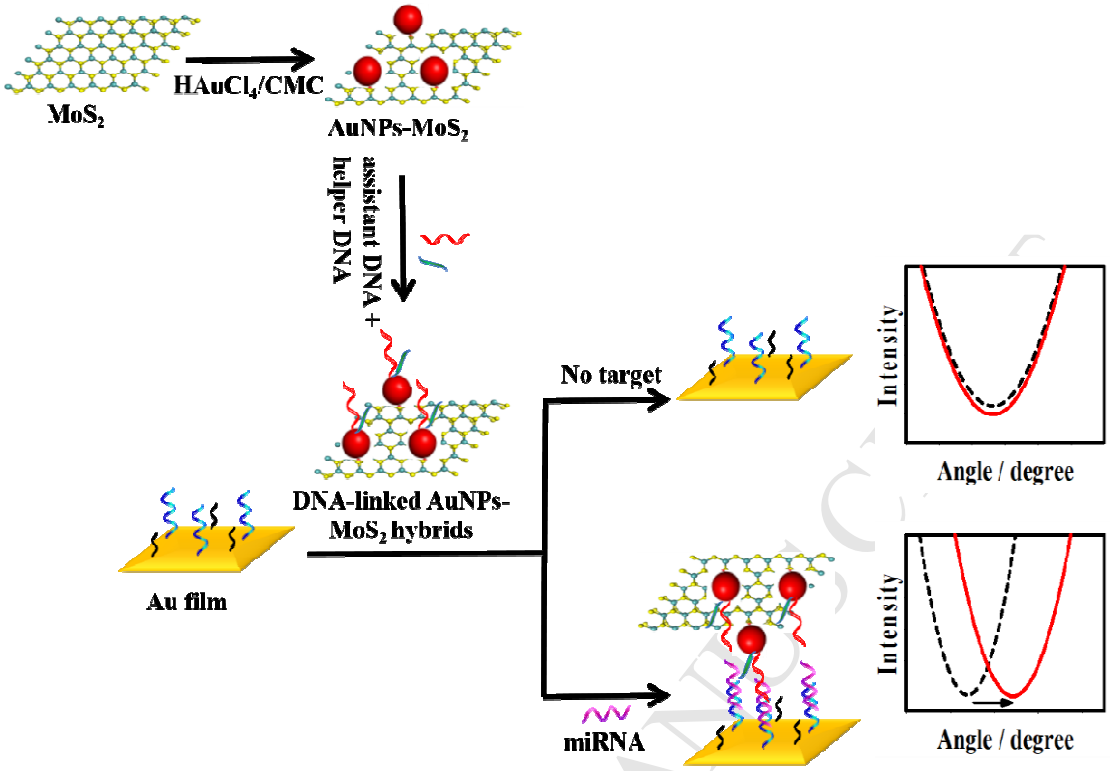

Fig. 1. The schematic illustration of the SPR biosensor based on the AuNPs-MoS_2 nanocomposites amplification.

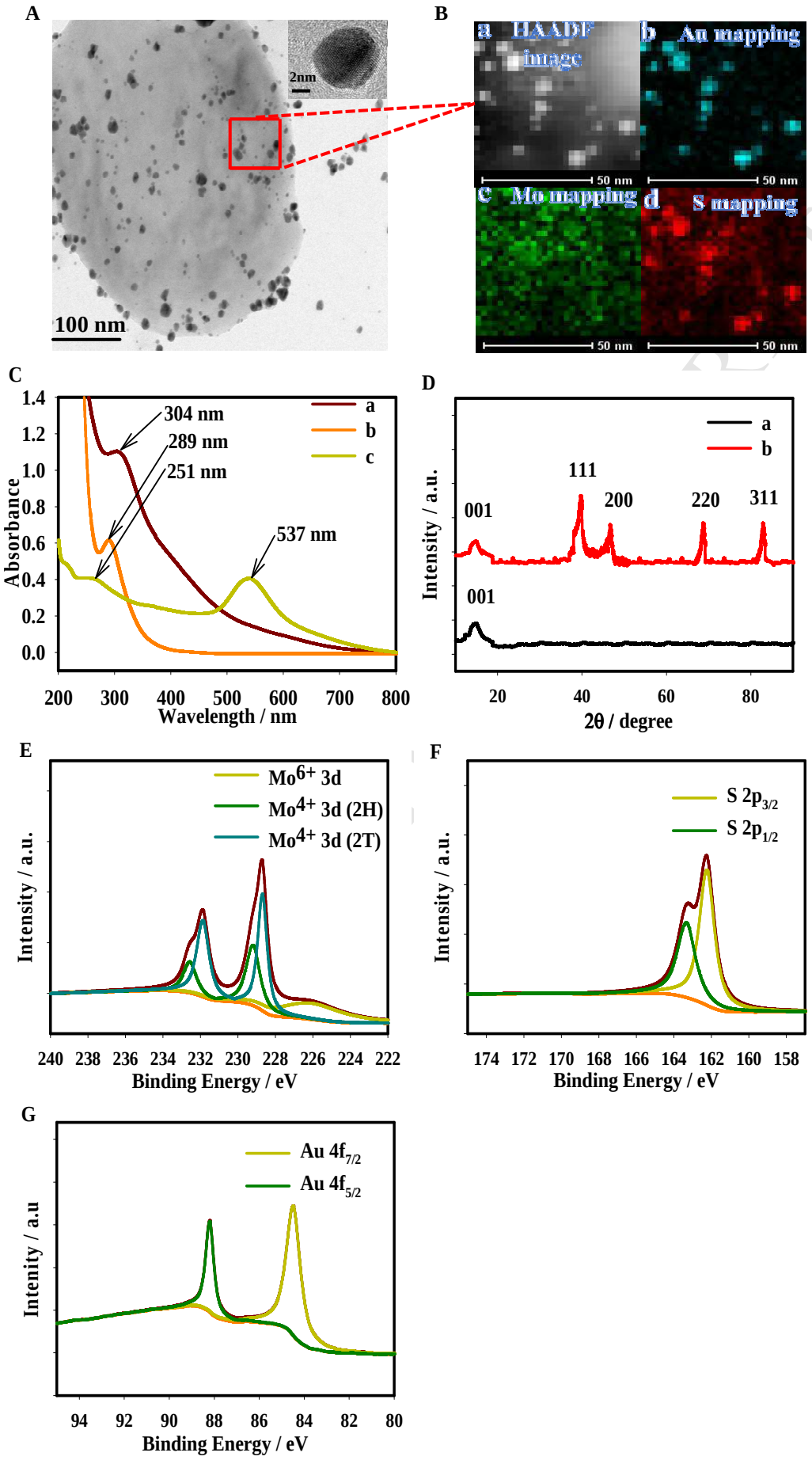
A
2nm
100 nm
B
a HAADF image
b Au mapping
c Mo mapping
d S mapping
50 nm
C
Absorbance
Wavelength / nm
304 nm
289 nm
251 nm
537 nm
a
b
c
D
Intensity / a.u.
2θ / degree
001
111
200
220
311
E
Intensity / a.u.
Binding Energy / eV
Mo6+ 3d
Mo4+ 3d (2H)
Mo4+ 3d (2T)
F
Intensity / a.u.
Binding Energy / eV
S 2p3/2
S 2p1/2
G
Intenity / a.u
Binding Energy / eV
Au 4f7/2
Au 4f5/2

Fig. 2. (A) TEM images of AuNP-MoS_2 nanocomposites. (B) Scanning transmission electron microscope-High angle annular dark-field (STEM-HAADF) image (a), Scanning transmission electron microscope-Energy dispersive X-ray spectroscopy (STEM-EDX) maps in Au Lα1 (b), S Kα1 (c), and Mo Kα1 (d) signals. (C) UV–Vis adsorption spectra of MoS_2 (a), $HAuCl_4$ (b) and AuNPs-MoS_2 nanocomposites (c). (D) XRD pattern of MoS_2 (a) and AuNPs-MoS_2 nanocomposites (b). X-ray Photoelectron Spectroscopy (XPS) spectra of AuNPs-MoS_2 nanocomposites in the Mo 3d (E), S 2p (F), and Au 4f (G) region.

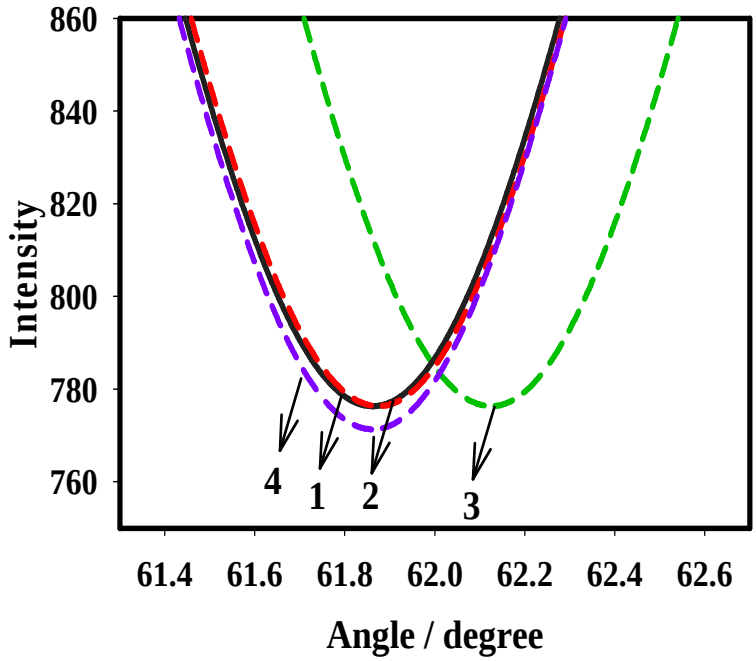

Fig. 3. SPR spectra of (1) capture DNA modified Au film; (2) hybridization with 50 pM miRNA-141; (3) reaction with the DNA-linked AuNPs-MoS_2; (4) regeneration.

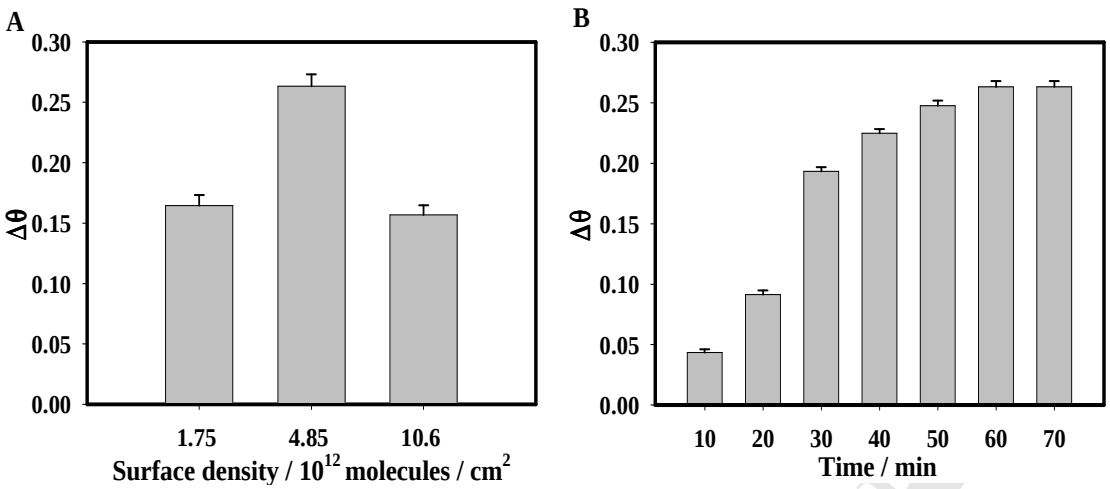

Fig. 4. Optimization of the experimental conditions. Effects of (A) surface density, (B) the incubation time of miRNA-141 (50 pM). The error bars represent the standard deviation of the three independent measurements. When one parameter changed, the others were under their optimal conditions.

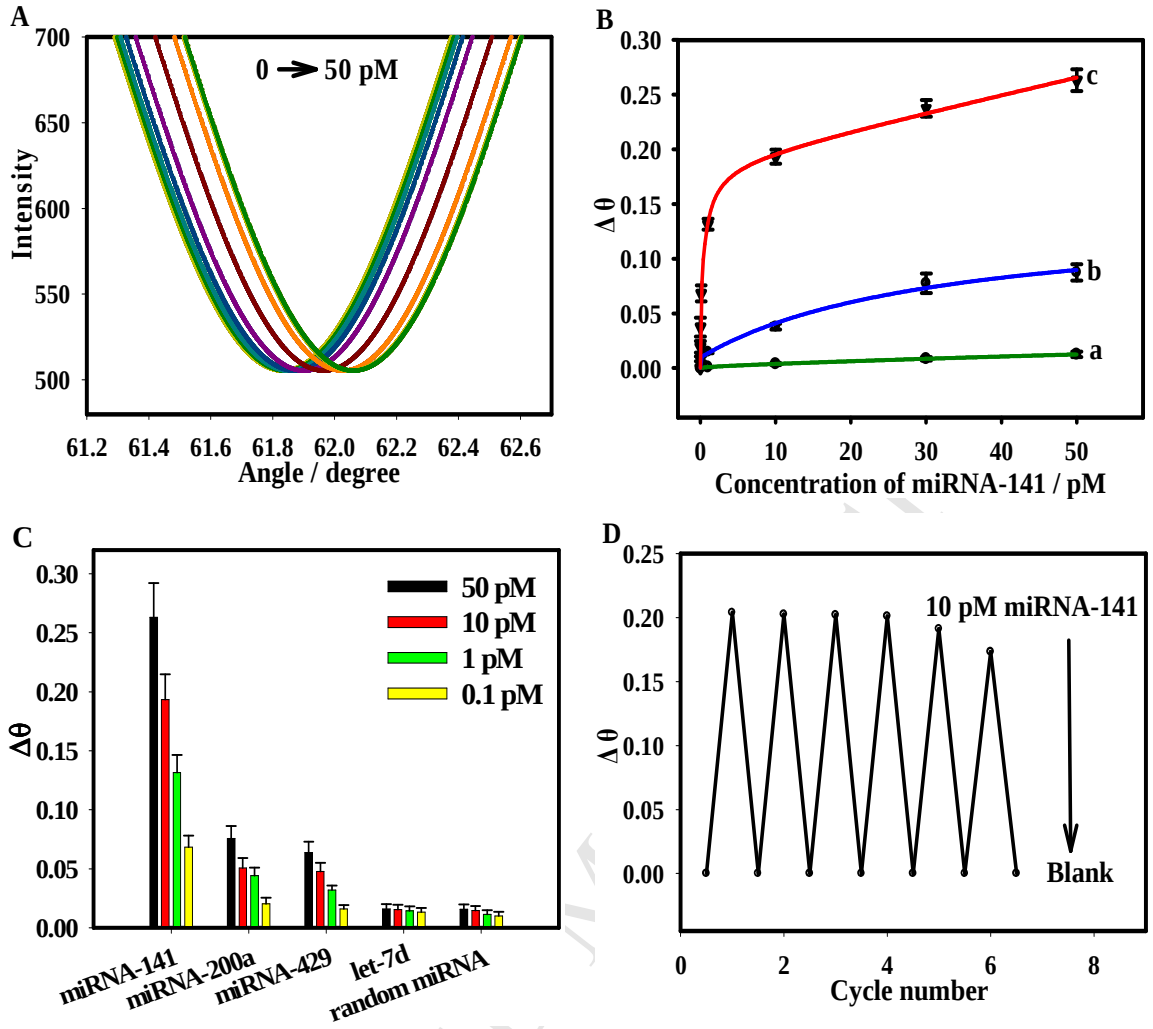

Fig. 5. (A) SPR spectra of different concentrations of miRNA-141. (B) The relationship between Δθ and miRNA-141 concentrations by using different sensing strategies. Error bars showed the standard deviation of measurement taken from three experiments. Direct hybridization measurement (a), AuNPs amplified SPR (b), and AuNPs/MoS_2-SPR (c). (C) Selectivity investigation of the AuNPs/MoS_2-SPR biosensor. Error bars showed the standard deviation of measurement taken from three experiments. (D) Reproducibility investigation of the AuNPs/MoS_2-SPR biosensor. The sensor chip was regenerated by introducing 0.1% SDS/10 mM NaOH for 5 min.

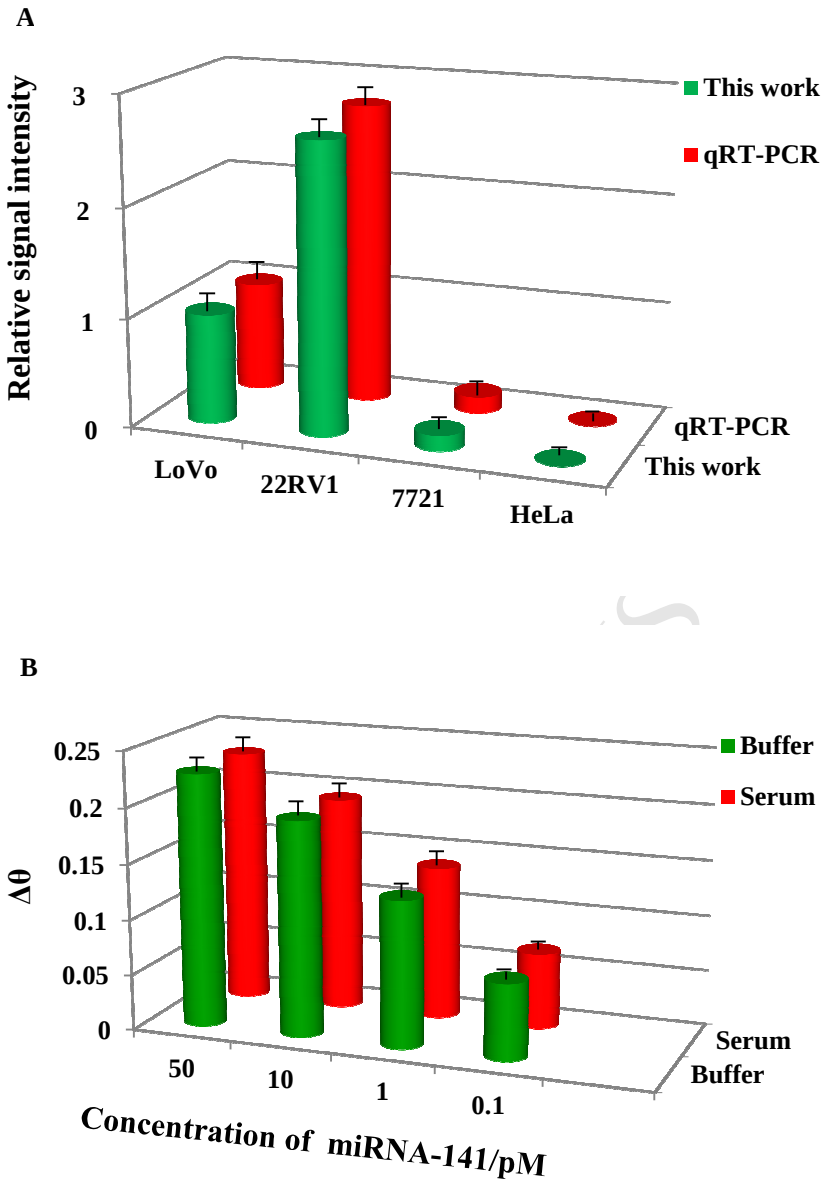

Fig. 6. (A) Paired comparison of the miRNA-141 levels detected in the total RNA isolated from four types of human cancer cell lines using qRT-PCR (red histogram) or the proposed biosensor (green histogram). Relative signal intensity was based on the expression ratio of miRNA-141 in the target cell lines versus that in the LoVo cell lines. (B) Detection of miRNA-141 in 10% human serum (red histogram) and buffer (green histogram). Error bars showed the standard deviation of measurement taken from three experiments.

Highlights

1. A sensitive SPR biosensor was firstly proposed based on AuNPs-MoS_2 nanocomposites.

2. This SPR platform for miRNA detection was executed in only two steps.

3. The AuNPs-MoS_2 nanocomposites were used as signal tags to enhance the SPR signal.

4. The SPR sensor exhibited high sensitivity with a detection limit of 0.5 fM.

5. This assay can be used for miRNA detection in complex samples.